Power Sharing Control Strategy of Multiterminal VSC-HVDC Transmission Systems Utilizing Adaptive Voltage Droop

Mohamed Abdelaziz Abdelwahed, *Student Member, IEEE*, and Ehab F. El-Saadany, *Senior Member, IEEE*

***Abstract*—This paper presents an adaptive droop-based power-sharing control strategy. The primary objective is to control the sharing of the active power transmitted by a multiterminal voltage-source converter based high voltage direct current network among a number of onshore ac grids or offshore loads based on the desired percentage shares. The shared power is generated by remote generation plants (e.g., offshore wind farms) or is provided as surplus from ac grids. The desired percentage shares of active power are optimized by the system operator in order to fulfil the active power requirements of the connected grids with respect to meeting goals such as supporting energy adequacy, increasing renewable energy penetration, and minimizing losses. The control strategy is based on two hierarchal levels: voltage-droop control as the primary controller and an optimal-power flow based secondary (supervisory) controller for selecting the optimal droop reference voltages. Based on the dc voltage transient and steady-state dynamics, a methodology for choosing the droop gains for droop controlled converters has been developed. The proposed control strategy has been validated through simulation on the CIGRE B4 dc grid test system. The results confirmed the flexibility and effectiveness of the power-sharing control provided by the new control strategy.**

***Index Terms*—Active power sharing control, CIGRE B4 test system, multiterminal voltage-source converter based high voltage direct current (MT VSC-HVDC) transmission, voltage-droop control.**

I. Introduction

THE aggregation and integration of offshore wind farms into AC grids can be accomplished with the use of MT VSC-HVDC transmission technology, which provides superior reliability, the ability to smooth wind energy fluctuations, flexible power transfer, and improved power-sharing control [1], [2]. In such multi-terminal HVDC network applications, voltage source converters (VSCs) offer a number of advantages over line-commutated converters (LCCs): black-start and reactive power support capabilities, simpler control, and active power flow reversal without a change in the DC voltage polarity [1].

Manuscript received January 12, 2016; revised April 19, 2016, July 23, 2016, and September 15, 2016; accepted September 19, 2016. Date of publication September 27, 2016; date of current version March 18, 2017. Paper no. TSTE-00035-2016.

M. A. Abdelwahed is with the Electrical and Computer Engineering Department, University of Waterloo, Waterloo, ON N2L3G1, Canada (e-mail: maabdelw@uwaterloo.ca).

Ehab El-Saadany is currently on leave with the Petroleum Institute, Abu Dhabi, UAE (e-mail: ehab@uwaterloo.ca).

Color versions of one or more of the figures in this paper are available online at http://ieeexplore.ieee.org.

Digital Object Identifier 10.1109/TSTE.2016.2614223

A number of power-sharing and voltage control methods have been proposed for MT VSC-HVDC systems. The base method, which is commonly used with parallel converters, is called the master-slave voltage control method: one master converter is responsible for regulating the voltage, while the other converters control their own power based on reference set-points sent by a central power-sharing controller. This method provides accurate power-sharing control based on a reference-sharing scheme, but only if the system is equipped with communication fast enough to send the active power set-point to the power-controlled converters periodically for any change in the generated power. Other shortcomings include the lower degree of reliability due to the probability of the single point failure of the master converter and the difficulty of expansion unless the master converter is rerated [3].

To reduce dependency on fast communication and increase system reliability, decentralized control strategies such as the voltage margin method (VMM) and fixed voltage-droop-based methods have been proposed. VMM is a modified version of the master-slave method whereby the voltage control operation is rotated in turn among different converters based on their local voltage and power levels [4], [5]. The main drawback of this method is the high amount of voltage oscillation resulting from the alternation [6], [7]. In a fixed-decentralized voltage-droop method, inspired by the power-frequency droop in AC systems, voltage regulation is distributed among a number of converters, with the active power being shared based on their droop characteristics. However, high accuracy of power sharing cannot be guaranteed because the output power sharing changes with the changing in the DC voltage level at the systems buses due to the wind power fluctuation, hence the droop parameters need to be updated [8].

To increase power-sharing accuracy, distributed voltage control methods are used, such as distributed direct voltage or adaptive droop-based control. The responsibility for voltage control is distributed among a number of converters by means of direct voltage control or droop-based control. The control parameters and set-points are periodically computed in a centralized controller and are then sent to different converters via low-speed communication. The distributed direct voltage control (DVC) method proposed in [9] employs a loss minimization OPF algorithm, which determines the voltage set-points of direct-voltage-controlled converters. However, due to line resistances, the accuracy of the power sharing and the optimality of the loss

minimization are affected by variations in wind power generation, especially when these variations are faster than the cycle for updating the voltage reference set-points. In addition, the voltage deviation and power sharing that occur after a converter outage are very sensitive to line resistances, and if communication is lost over a long period, system stability will be affected, and the system voltage may violate recommended limits.

Because it provides droop-control stability in case of the communication loss, an adaptive voltage-droop method is used for overcoming the disadvantages of the DVC technique. The virtual resistance of the droop gain also reduces the sensitivity of the power sharing to line resistances so that the accuracy of the power sharing is increased. However, previous studies that investigated power sharing using this method in MT HVDC networks included consideration of only small-scale systems with few buses and converters, making them highly system-dependent [3], [6], [10]. Applying such algorithms to large-scale systems with meshed or ring topologies is more complex [11], and their expansion is not easy. Furthermore, in [5], [12], [13], the no-load voltage of the onshore VSCs droop controllers are optimized such that the losses in the HVDC transmission cables or the VSCs stations are minimum. However, loss minimization as a power-sharing objective might not achieve desired power shares preferences of each connected AC grid. These preferences can be supporting energy adequacy, increasing wind energy penetration, or maximizing converter loadability. An additional factor is that droop gain values affect both DC voltage dynamics and the accuracy of the power sharing [14], [15]. Despite these considerations, previous researchers did not take into account DC voltage transient dynamics in their power-sharing control algorithms. Although the authors of [14], [16], and [17] proposed methodologies for selecting droop gains based on consideration of DC voltage dynamics, their methods relied on the calculation of a factor to be multiplied by all droop gains predetermined from power-sharing control algorithms, in order to achieve optimal DC voltage dynamics without the violation of any constraints. Such methods could affect the accuracy of the power-sharing control. According to the available headroom of each converter station, the algorithm proposed in [18] adapts the droop gains, which is preselected respect to the converter rating not from a power-sharing control algorithm, to share the burden after a converter outage considering the system stability. Without considering the power-sharing control, the droop parameters are optimized in order to not compromise the AC system stability after a converter outage and abrupt power set-points changing [19]. At the DC micro-grid level, an improved droop control for load current sharing of distributed generators (DGs) is proposed in [20]. This droop control improvement aims at increasing the accuracy of the load current sharing by modifying the droop controller reference voltage as a function of the average DC voltage and current, which are broadcasted among the DGs using low-bandwidth communication, while keeping the droop gains fixed.

This paper provides a power-sharing control strategy that utilizes an adaptive voltage-droop scheme, in which the voltage-droop parameters are optimally selected as a means of achieving accurate power sharing based on the desired shares, which are optimized in advance by the system operator in order to fulfil the active power requirements of the connected AC grids, while also including consideration of the DC voltage dynamics, including transient and steady-state performance.

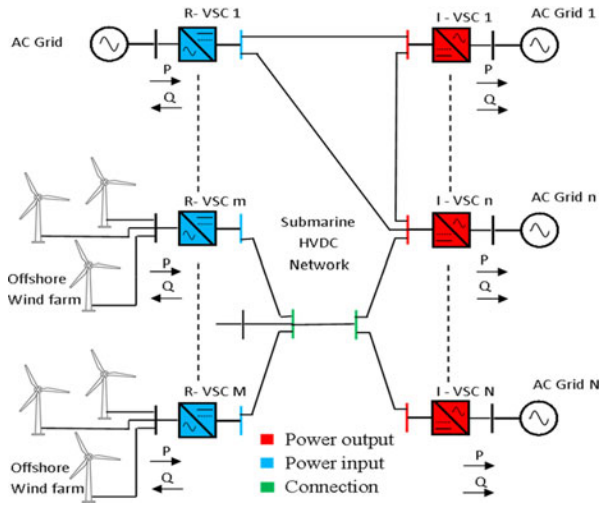

Fig. 1. MT VSC-HVDC network.

The remainder of this paper is organized as follows: Section II illustrates the control structure of MT VSC-HVDC networks. The derivation of both state-space and steady state models is explained in Section III. Section IV presents the proposed power sharing control strategy including the proposed methodology for droop-gain selection and the proposed OPF-based power-sharing control algorithm. The simulation results are reported in Section V, and conclusions are provided in Section VI.

II. MT VSC-HVDC Network Control

In an offshore MT VSC-HVDC transmission system (Fig. 1), the DC network connects offshore wind farms and onshore AC grids through submarine HVDC cables and interfacing VSCs. Bidirectional DC-DC converters are used for connecting HVDC networks characterized by differing DC voltage levels so that active power can be exchanged between them. The connection topologies of the HVDC networks differ depending on economical, geographical, and technical factors [11], [20]. Their system buses can be classified as three types: power input, power output, and connection buses to which no converter is connected. Power input buses are connected to the converters that deliver active power to the HVDC transmission network from offshore wind farms or AC grids that have exporting power. Power output buses are connected to the converters that absorb active power from the HVDC network. Connection buses have no converters connected to them. The control strategy for an MT VSC-HVDC network is a two-level control structure in hierarchal form with a primary and a secondary (supervisory) level.

A. Primary Level

At the primary control level of the system converters (Figs. 2 and 3), a decoupled current controller controls the real and imaginary current components independently [22]. Its control structure can be divided into two main stages: the inner current control loop and the outer loops [5], [6], [8], [25].

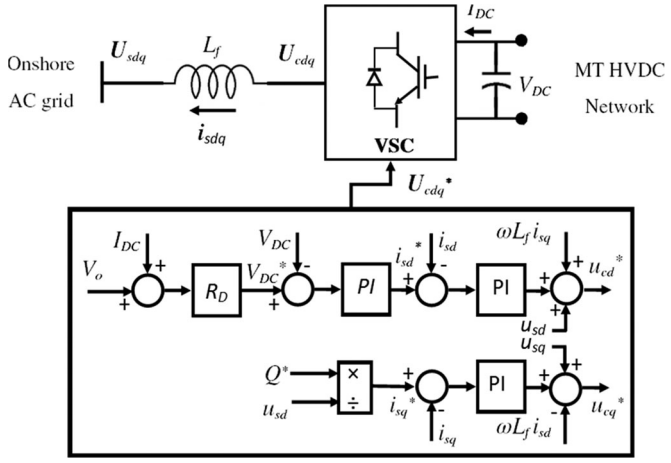

Fig. 2. Local controller of an output VSC.

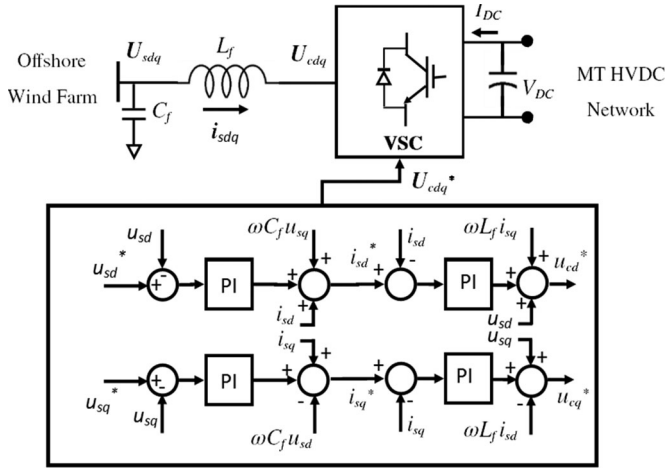

Fig. 3. Local controller of a wind farm VSC.

The inner loop is a PI controller responsible for controlling the decoupled AC currents i_{sdq} by generating the reference voltage values of the converter $U^*_{C_{\mathrm{dq}}}$ based on equation (1):

$$U^*_{C_{\mathrm{dq}}} = \left(K_p + \frac{1}{s}K_i\right)\left(\boldsymbol{i}^*_{s_{\mathrm{dq}}} - \boldsymbol{i}_{s_{\mathrm{dq}}}\right) + wL\boldsymbol{i}_{\mathrm{sdq}} + \boldsymbol{U}_{S_{\mathrm{dq}}} \tag{1}$$

where K_p and K_i are the proportional and integral controller gains; i_{sdq} and $\boldsymbol{i}^*_{\mathrm{sdq}}$ are the actual and reference values of the VSC's AC current dq components; ω is the frequency; L is the inductance of the AC filter; and $U_{S_{\mathrm{dq}}}$ are the dq-components of the AC voltage at the point of common coupling.

The outer loops define the control mode of the converter, which produces the decoupled reference currents $\boldsymbol{i}^*_{\mathrm{sdq}}$ for the inner loop. The outer loops contain two different PI controllers: one for the d-axis and the other for the q-axis. One of the active power, the DC current, or the DC voltage is controlled by controlling the d-axis current. On the other hand, the q-axis current control is used for controlling either the reactive power or the AC voltage at the point of common coupling (PCC) [15].

The outer control loop of the power output grid-side converters is a DC voltage controller, see Fig. 2, and its DC voltage set-point V_i^* is calculated from the droop control, using (2), so that the active power absorbed by the converter at the i^{th} node can then be defined by (3).

$$V_i^* = V_{o_i} + R_{D_i} I_i \tag{2}$$

$$P_i = V_i I_i = \frac{V_i}{R_{D_i}}(V_i^* - V_{o_i}) \tag{3}$$

where I_i and P_i are the input DC current and active power of the i^{th} converter, respectively; V_{o_i} and R_{D_i} are the no-load voltage and the droop gain of converter *i*, respectively; and V_i is the DC voltage at node i. In this case, the output converters share the power/current based on their droop-control parmeters R_D and V_o.

In power input grid-side converters, the outer loop is a constant active power controller that has the same structure as that shown in Fig. 2 but with the DC voltage V_{DC} replaced by the active power *P*; the reference power is set based on the surplus power available from the AC grid. Otherwise, the structure of the primary controller of the offshore wind farm converter is as illustrated in Fig. 3; its purpose is to control the AC voltage and frequency of the wind farm AC grid. The active power flowing through them is based on the generation from the wind turbines. In steady state analysis, wind farm converters can thus be considered constant power.

B. Supervisory Level

The supervisory controller calculates the droop-control parameters of the output converters. These parameters are selected in order to achieve two objectives: the provision of accurate sharing of the input power based on predefined percentage shares, and the enhancement of the DC voltage dynamics. An additional goal is to ensure that the DC voltage level at any bus is maintained within limits.

III. Network Model

Implementing the proposed control strategy requires steady state and dynamic state-space models of the MT VSC-HVDC network. For a system with N power output buses, M power input buses, and P connection buses, both models are derived as explained in the following subsections.

A. Dynamic State-Space Model

In this work, to study the DC voltage transient as a function of the droop gains, a state-space model of the MT HVDC system is derived for the droop-gain selection. The dynamics associated with the converter switching and the harmonics are not considered. Thus, the VSCs are represented by their average models, in which the AC side is modeled as three AC sources with an inductor and a resistor in series per phase, while the DC side is modeled as a current source with a capacitor in parallel [14], [26], as shown in Fig. 4. However, the derivation of the system model are based on two main assumptions. First, all onshore AC grids are considered stiff grids. Second, the inner and the outer control loops of the onshore VSCs are assumed to be well designed and have a first or second order filter response. According to these assumptions, the AC voltage at the point of

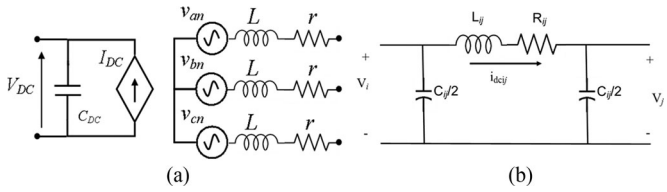

Fig. 4. Average value model of the (a) VSC and (b) DC link.

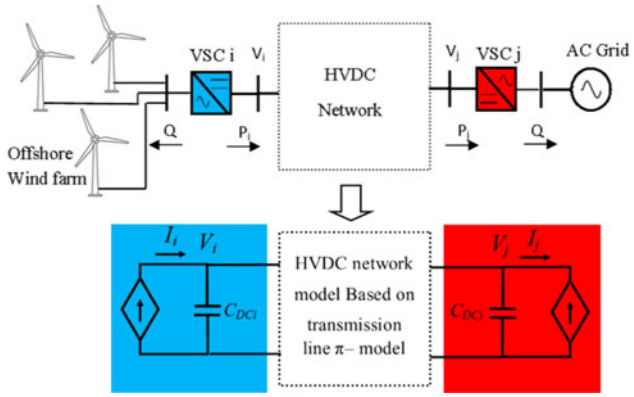

Fig. 5. Average model of an MT VSC-HVDC system.

common coupling of the onshore VSC is not affected by the power flow through the converter. Furthermore, in the offshore wind farms, the VSC controls the frequency and the AC voltage. The AC voltage level at the wind farm VSC terminals is controlled regardless of the amount of power flowing through the converter. In addition, according to the small signal stability analysis in [18], the critical modes, i.e., the most right eigenvalues, are mostly associated with the DC network and the droop controller states. Hence, the DC voltage dynamics are further influenced by the DC network parameters and the droop gains. Accordingly in this work, each VSC is represented by a current source in parallel with a DC capacitor. This representation is also used for droop controlled DGs in DC microgrids [20]. Moreover, a π model is used for modeling the transmission lines. Fig. 5 represents an example of the MT VSC-HVDC average value model.

The DC current values of the droop-controlled VSCs can be calculated using (2), and for any i^{th} power input VSC, its output DC current value I_i is proportional to its incoming active power P_i, assuming that its voltage V_i always remains close to its nominal value [14]. The current value is hence

$$I_i = \frac{P_i}{V_i} \tag{4}$$

Equations (5) to (8) represent the dynamic differential equations for the system.

1) Line Equations:

$$\frac{d}{dt}\, I_{\mathrm{ij}} = -\frac{R_{\mathrm{ij}}}{L_{\mathrm{ij}}}\, I_{\mathrm{ij}} + \frac{1}{L_{\mathrm{ij}}}\, (\mathrm{V}_i - \mathrm{V}_j) \tag{5}$$

where R_{ij} and L_{ij} are the resistance and inductance of the DC link between nodes *i* and *j*, respectively; V_i and V_j are the DC voltages of nodes *i* and *j*, respectively; and I_{ij} is the current flows from node *i* to node *j*. all DC line connecting the DC buses are numbered from 1 to T in the state space model, where T is the total number of the DC lines. Thus, they are numbered from I_{l_1} to I_{l_T} .

2) Bus Equations: For power output (droop-based buses), the closed loop transfer function of the DC voltage controller, in which the reference voltage V_i^* is calculated by the droop equation (1), is assumed to have a first order filter response as in (6*)*

$$\frac{V_i(s)}{V_i^*(s)} = \frac{1}{Ts+1} \tag{6}$$

where T is the time constant of the DC voltage control loop. From (6) the dynamic differential equation of the DC voltage controller is as follows

$$V_i^* = T\frac{d}{dt}\, V_i + V_i \ , \ \forall i \in N \tag{7}$$

Using equation (1) and (7), the dynamic equation of the power output buses is

$$\frac{d}{dt}\, V_i = \frac{-G_{D_i}}{C_i + G_{D_i}\, T}\, (V_i - V_{o_i}) + \frac{1}{C_i + G_{D_i}\, T} \sum_{j \in n_b} I_{\mathrm{ij}}, \quad \forall i \in N \tag{8}$$

For power input buses,

$$\frac{d}{dt}\, V_i = \frac{1}{C_i}\, I_i + \frac{1}{C_i} \sum_{j \in n_b} I_{\mathrm{ij}} \quad \forall\, i \ \in M \tag{9}$$

For connection buses,

$$\frac{d}{dt}\, V_i = \frac{1}{C_i} \sum_{j \in n_b} I_{\mathrm{ij}}\, \forall\, i \ \in P \tag{10}$$

$$C_i = C_{\mathrm{dci}} + \sum_{j \in n_b} C_{\mathrm{ij}}, \forall\, i \ \in N_B \tag{11}$$

$$G_{D_i} = \frac{1}{R_{D\,i}} \tag{12}$$

where N_B, N, M, and P are the sets of the total, output, input, and connection buses, respectively; n_{b} is the set of buses connected to bus *i*; $\mathrm{I_i}$ is the input or output DC current at the i^{th} node; and V_{oi} and R_{Di} are the droop-control parameters of the converter at the i^{th} node.

From equations (8), (9) and (10), the state-space model can be represented as

$$\begin{aligned} \dot{\boldsymbol{x}} &= \boldsymbol{A}\, \boldsymbol{x} + \boldsymbol{B}\, \boldsymbol{u} \\ \boldsymbol{y} &= \boldsymbol{C}\, \boldsymbol{x} \end{aligned} \tag{13}$$

where

$$\begin{aligned} \boldsymbol{x} &= [I_{l_1} \ldots I_{l_T} \ \ V_1 \ldots V_{N+M+P}]^T \\ \boldsymbol{u} &= [V_{o_1} \ldots V_{o_N} \ \ldots \ I_{N+1}\ I_{N+2} \ldots \ I_{N+M}]^T \\ \boldsymbol{y} &= [V_1 V_2 \ldots V_{N+M}\ ]^T \end{aligned} \tag{14}$$

To find a direct relation between the voltage deviation at the input buses and the variation in the input currents, the state-space

model is modified through linearization as follows:

$$\begin{aligned}\Delta \boldsymbol{x} &= \boldsymbol{A}\,\Delta \boldsymbol{x} + \bar{\boldsymbol{B}}\Delta \boldsymbol{u}\\ \Delta \boldsymbol{y} &= \boldsymbol{C}\quad \Delta \boldsymbol{x}\end{aligned} \tag{15}$$

where

$$\begin{aligned}\Delta \boldsymbol{x} &= [\Delta i_{l1}\ \ldots\ \Delta i_{lT}\ \Delta V_1 \ldots\ \Delta V_{N+M+P}]^T\\ \Delta \boldsymbol{u} &= [\Delta I_{N+1}\ \Delta I_{N+2} \ldots..\ \Delta I_{N+M}]^T = \Delta \boldsymbol{I}\\ \Delta y &= [\Delta V_{N+1} \Delta V_{N+2} \ldots..\Delta V_{N+M}\ ]^T = \Delta \boldsymbol{V}\end{aligned}$$

$$\bar{\boldsymbol{B}} = \begin{bmatrix} \frac{1}{C_{N+1}} & \cdots & 0 \\ \vdots & \ddots & \vdots \\ 0 & \cdots & \frac{1}{C_{N+M}} \end{bmatrix} \tag{16}$$

where $\Delta \boldsymbol{I}$ is the vector of the input bus incoming current, $\Delta \boldsymbol{V}$ is the vector of the input bus voltage, and R_l and L_l are the resistance and inductance of the DC line.

B. Steady-State Model

To implement the OPF algorithm responsible for calculating the optimal droop-control reference voltages, the steady state model of the MT VSC-HVDC network is derived. In this model, DC transmission lines are assumed to be purely resistive. Equation (17) is the general load flow equation at bus *i* [27]:

$$G_{\rm ii} V_i^2 - V_i \sum_{j \in n_b} C_{\rm ij} {\rm V}_j - P_i = 0\ \ \forall\, i\ \in N_B\ \ j \in n_b \tag{17}$$

where $G_{\rm ij} = 1/R_{\rm ij}$ is the line conductance between buses *i* and *j*; P_i is the net input power of the converter *i* (from bus *i* to converter *i*); V_i and V_j are the DC voltages of the $i^{\rm th}$ and $j^{\rm th}$ buses, respectively; and

$$G_{\rm ii} = \sum_{j \in n_b} G_{\rm ij}\ \forall\, i\ \in N_B \tag{18}$$

For the three types of buses in the network (power output buses, power input buses, and connection buses), the power flow equations are as follows.

1) Power Output Buses: The buses, which are connected to the current droop-control converters, have a droop equation (2). Modifying the equation as in (12) and substituting it into (17) gives the following droop equation for bus *i*:

$$G_{\rm ii} V_i^2 - V_i \sum_{j \in n_b} G_{\rm ij} V_j + G_{\rm Di} V_i\,(V_i - V_{oi}) = 0 \quad \forall\, i\ \in N \tag{19}$$

2) Power Input Buses: Equation (20) is the load flow equation for the bus that is connected to a rectification mode converter and whose output power is controlled through a constant power controller. At steady state, the output power of that converter equals its reference active power setting.

$$G_{\rm ii} V_i^2 - V_i \sum_{j \in n_b} G_{\rm ij} V_j - P_i^* = 0\ \forall\, i\ \in M \tag{20}$$

where P_i^* is the active power of the $i^{\rm th}$ power input converter.

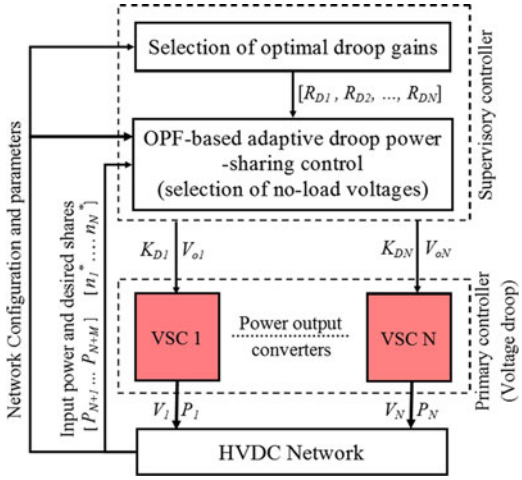

Fig. 6. Structure of the proposed MT VSC-HVDC power-sharing controller.

3) Connection Buses: The connection bus is the bus that is not connected to any converter; the following is the load flow equation at connection bus *i*:

$$G_{\rm ii} V_i^2 - V_i \sum_{j \in n_b} G_{\rm ij} V_j = 0 \quad \forall\, i\ \in P \tag{21}$$

IV. Proposed Power-Sharing Control Strategy

The proposed power-sharing controller is a two-level hierarchal controller. Its layout (Fig. 6) includes a high-level supervisory centralized controller that computes and sends the optimal droop parameters (i.e., R_D and V_o) to the primary controller of the power output converters. In order to achieve the main two objectives of the control strategy, which are the DC voltage dynamics enhancement and the power sharing control accuracy improvement, the supervisory controller selects the optimal droop parameters in two steps following receipt of the required data: the DC network configuration and parameters, the available input power, and the desired power shares. At the beginning, the optimal droop gains of the droop-controlled converters (i.e., output converters) are selected once using the methodology explained in subsection IV-A. However, this process should be repeated for each change in the HVDC network configuration (i.e., a change in the number of converters due to a converter entering or exiting the service, or a change in the DC network topology because of the connection or disconnection of DC links).

After selecting the droop gains, the supervisory controller then chooses the optimal values for the droop reference voltage using the OPF algorithm explained in next subsection IV-B. The data required for performing this process is the power available to be input to the HVDC network, specifically, the generation from connected wind farms, which can be obtained from the forecasted data, and/or the surplus active power that can be imported from connected AC grids. An additional requirement is the desired percentage shares, which is set by the operator based on a variety of scenarios. For example, in a priority-sharing scheme, one of the power output converters

would be assigned the priority of absorbing a specific amount of active power, while the other converters would share the extra power. The power shares may change based on the power trading that takes place during the day. This process is repeated periodically so that the percentage shares is maintained at the desired value. The updating rate of the droop parameters is set based on the the rate of change of the wind power. Any deviation in the input power produces a deviation in the output buses voltage level, which in turn affects the power sharing accuracy. Hence, the faster the update rate, the better the power sharing accuracy given reliable communication speed.

A. Methodology for Selecting the Optimal Droop Gains

The value of the droop gain affects the system DC voltage dynamics as a result of the change in the DC power input to the system (i.e., active power that is delivered by wind farm VSCs). As revealed in the simulation results presented below, changing the droop gain value affects both transient and steady state DC voltage dynamics. Increasing the droop gains tends to improve the transient response of the DC voltage, and the accuracy of the power sharing increases as the sensitivity of the sharing to transmission line resistance decreases; however, the steady state voltage level at the DC network buses increases and may exceed the upper voltage limits (+5%) [14]. The small-signal stability analysis expressed in Section V confirms that the system is stable for any positive droop gain value. When the droop gains are increased, all of the eigenvalues become increasingly negative without any effect on the damping frequency.

The objective of the proposed methodology is the selection of the optimal droop-gain values that will lead to the best possible DC voltage transient response to variations in input power or an output converter outage, without changes to the system parameters and without violating the voltage limits.

To find a relation between the steady state voltage deviation and input power variations as a function of the droop gains, the transfer matrix of the system, which is a function in the droop gains, as indicated in (22), and the steady state gain matrix (23) [28] can be determined as follows:

$$\boldsymbol{G}(\boldsymbol{s}) = \frac{\Delta \boldsymbol{V}(\boldsymbol{s})}{\Delta \boldsymbol{I}(\boldsymbol{s})} = \bar{\boldsymbol{C}}(\boldsymbol{s}\boldsymbol{I} - \boldsymbol{A})^{-1}\bar{\boldsymbol{B}} \tag{22}$$

$$\boldsymbol{H} = \lim_{\mathrm{s}\to 0} \boldsymbol{G}(\boldsymbol{s}) \tag{23}$$

The steady state voltage deviation $\Delta \boldsymbol{V}_{\mathrm{ss}}$ due to a change in the input current can then be calculated as follows:

$$\Delta \boldsymbol{V}_{\mathrm{ss}} = \boldsymbol{H} \cdot \Delta \boldsymbol{I}_{\mathrm{ss}} \tag{24}$$

The maximum possible voltage deviation in the system is found from

$$\Delta V_{\max} = ||H \cdot \Delta \boldsymbol{I}_{\max}||_{\infty} \tag{25}$$

where $\Delta \boldsymbol{I}_{\max} = [\, \Delta I_{N+1\max}\ \Delta I_{N+2\max} \ldots .. \Delta I_{N+M\max}]^T$ is the vector containing the maximum possible changes in the input currents.

To achieve the objective of this methodology, the real part absolute value of the least negative eigenvalue of the transition matrix **A** is maximized, thus guaranteeing the minimization of the real part of all of the eigenvalues and hence enhancing the maximum overshoot and settling time of the voltage.

The optimal droop gain selection optimization problem is formulated as in (26) and (27):

$$\max_{z}(|\sigma_{\min}(z)|) \tag{26}$$

where $\sigma_{\min}$ is the least negative real part of the system eigenvalues. The objective function is subject to the following constraints:

$$\begin{aligned} \Delta V_{\max}(z) &\le V_{\mathrm{DC}\max} - V_{o_{\max}} \\ \Delta V_{\max_{\mathrm{out}\,i}}(z) &\le V_{\mathrm{dc}\max} - V_{o_{\max}},\ \forall\, i \in N \end{aligned} \tag{27}$$

where z is the vector of the droop-controlled VSC droop gains as follows:

$$z = [R_{D_1} \ldots R_{D_N}]^T, \tag{28}$$

$V_{o_{\max}}$ is the largest no-load voltage value, which becomes the upper bound of the voltage reference values in the DC OPF algorithm, as explained in the next section, and $\Delta V_{\max_{\mathrm{out}\,i}}(z)$ is the steady state maximum DC voltage deviation as a result of the disconnection of the output converter *i*. The value of $\Delta V_{\max_{\mathrm{out}\,i}}(z)$ is calculated for all possible single output converter outage scenarios by using equations (22) to (25), but with the value of the disconnected converter *i* droop gain is set to $G_{D_i} = \frac{1}{R_{D_i}} = 0$.

The value of $V_{o_{\max}}$ is selected to be greater than the mid-point between $V_{\mathrm{dc}_{\max}}$ and $V_{\mathrm{dc}_{\min}}$ as in (29). Hence, when the power flow direction is reversed in an output converter the DC voltage will not violate the $V_{\mathrm{dc}_{\min}}$ at the selected droop gains, which is selected to prevent the DC voltage from exceeding the upper limit at the maximum power, i.e. rated power.

$$V_{o_{\max}} > \frac{V_{\mathrm{dc}_{\max}} + V_{\mathrm{dc}_{\min}}}{2} \tag{29}$$

In optimal droop gain selection methodology, the selection of the droop gain can be adjusted by changing the values of $V_{o_{\max}}$ or $\Delta \boldsymbol{I}_{\max}$. Selecting a lower $V_{o_{\max}}$ value results in a higher droop gain without violation of the voltage limits, which increases the accuracy of the power sharing. For extreme variations, the $\Delta \boldsymbol{I}_{\max}$ vector elements are selected to represent the maximum change in the current and thus equal the twice rated current for the onshore grids VSCs or the rated current for wind farm VSCs. However, under normal operating conditions, fewer variations in active power occur because it does not change from zero to the rated value. Hence, $\Delta \boldsymbol{I}_{\max}$ elements can be selected as the maximum possible change in the current during a specific period based on forecasted data. In this case, the droop-gain selection step could be repeated periodically whenever the value of $\Delta \boldsymbol{I}_{\max}$ changes.

B. OPF-Based Adaptive Droop Power-Sharing Control

The objective of the algorithm is the selection of optimal droop-control reference voltages for the output converters in order to achieve accurate active power sharing based on optimized-predetermined desired shares. The algorithm is formulated as expressed in (30) to (38):

The objective function is the minimization of the root of the average squared errors:

$$\min_{v} \sqrt{\frac{\sum_{i=1}^{N} e_i(v)^2}{N}} \tag{30}$$

where $e_{\rm i}$ is the difference between a) the desired percentage share $n_{\rm i}^*$, which is set by the operator in order to define the percentage share of the total input power of each output converter, and b) the actual share of the power output by the $i^{\rm th}$ VSC, as calculated by (31); $\boldsymbol{v}$ is the vector of the output reference (no-load) voltages of the converters and the DC voltages at all buses, $\boldsymbol{v} = [V_{o_1} \ldots V_{o_N} \; V_1 \ldots V_N]^T$:

$$e_i = n_i^* - \frac{P_i}{P_G - P_{\rm loss}} \tag{31}$$

where P_i is the power output through the $i^{\rm th}$ VSC that can be calculated from (3). $P_{\rm G}$ is the total power input to the HVDC network, i.e., the summation of the reference power values of the constant power-controlled converters (32), and $P_{\rm loss}$ is the total transmission loss from the DC network, as computed by (33) and (36), respectively:

$$P_G = \sum_{\forall j \in M} P_j^* \tag{32}$$

$$P_{\rm loss} = \sum_{\forall\, i \in N_B} \sum_{\forall\, j \in N_B} G_{\rm ij}(V_i - V_j)^2 \tag{33}$$

The objective function is subject to the following constraints:

$$g(\boldsymbol{v}, \boldsymbol{P}) = [g_1 \ldots g_{NB}]^T = 0 \tag{34}$$

$$V_{dc_{\min}} \le V_i \le V_{{\rm dc}_{\max}}, \qquad i \in N_B \tag{35}$$

$$V_{o_{\min i}} \le V_{o_i} \le V_{o_{\max}}, \quad i \in N \tag{36}$$

$$|P_i| \le P_{i_{\max}}, \quad i \in N \cup M \tag{37}$$

$$I_{{\rm dc}_k} \le I_{{\rm dc}_{k\max}}, \quad k \in L \tag{38}$$

where L is the set of DC network links. Equation (34) shows the nonlinear equality constraints, where, g_1 to g_N is represented by (19), g_{N+1} to g_{N+M} equals (20), and (21) shows the value of g_{N+M+1} to $g_{\rm NB}$. In the non-equality constraints (35) to (38), $V_{{\rm dc}_{\min}}$ and $V_{{\rm dc}_{\max}}$ are the lower and upper DC voltage terminal limits, respectively; $P_{i_{\max}}$ indicates the maximum power of the $i^{\rm th}$ converter; and the maximum DC current capacity of the link k is denoted by $I_{{\rm dc}_{k\max}}$, and $V_{o_{\min i}}$ is the minimum no-load voltage value for the converter i. The value of $V_{o_{\min i}}$ is calculated for every output converter by (39) in order to avoid the violation of the lower DC voltage limit after any power flow direction reversal in the output converter i.

$$V_{o_{\min_i}} = V_{{\rm dc}_{\min}} + \frac{R_{D_i} P_{{\rm rated}_i}}{V}_{{\rm dc}_{\min}} \quad \forall\, i \in N \tag{39}$$

where R_{D_i} and $P_{{\rm rated}_i}$ are the droop gain and the rated active power of the i^{th} output converter.

This optimal power flow optimization problem, which is nonlinearly constrained, is solved using a trust region reflective optimization algorithm [29].

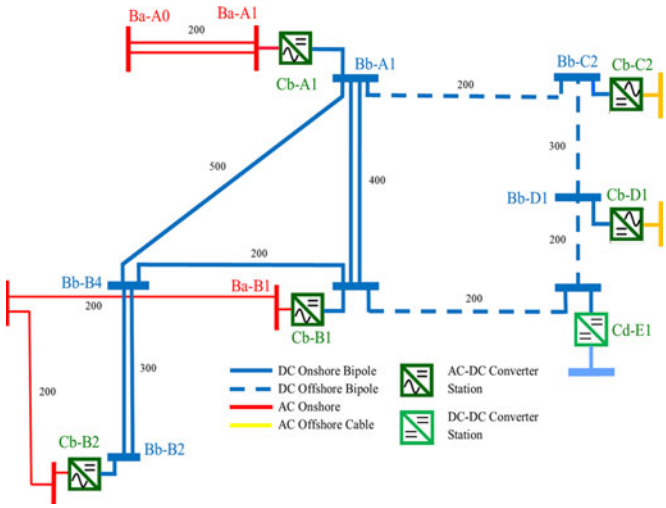

Fig. 7. CIGRE B4 DC grid test system (DCS3) [25].

TABLE I
CONVERTER STATION DATA PER POLE

	Cb-A1	Cb-B1	Cb-B2	Cb-C2	Cb-D2	Cd-E1
$S_{\rm rated}$ [MW]	1200	1200	1200	400	800	1000
r [Ω]	0.403	0.403	0.403	1.210	0.605	1.92
L [mH]	33	33	33	98	49	800
$C_{\rm f}$ [μF]	–	–	–	2	2	–
$C_{\rm dc}$ [μF]	450	450	450	150	300	7.8125

V. SIMULATION RESULTS

The proposed control strategy was validated on the CIGRE B4 DC grid test system, which includes two onshore AC grids and four offshore AC grids (wind farms). The AC grids are connected by three HVDC grids: DCS1, DCS2, and DCS3, with seven VSCs overall. Detailed system data can be found in [30].

In this work, a bipolar DCS3 meshed HVDC grid (Fig. 7) was used as a test system, with two offshore wind farms, D and C, connected to onshore AC grids A and B through overhead and cable DC links. AC grid B has two VSCs that interface with DCS3: Cb-B1 and Cb-B2 at buses B1 and B2, respectively. AC grid A and wind farms D1 and C2 are connected to the DCS3 DC grid through VSCs: Cb-A1 at bus B4, Cb-C2 at bus B5, and Cb-D1 at bus B6. DCS3, which is a bipolar ± 400 kV DC grid, is connected with the symmetrical unipolar ± 200 kV DCS2 DC grid through the bidirectional DC-DC converter Cd-E1 in order to transfer power between them. The converter parameters and line data are as stated in Table I and Table II, respectively. Per unit data were calculated based on common base values, as follows: $S_{\rm base} = 1200$ MW, $V_{\rm dcbase} = 400$ kV, onshore and offshore $V_{\rm ACbase} = 120$ kV, The DC voltage limits of the system were set to be $+5\%$ and -10%.

Based on predefined active power sharing scheme, converters Cb-B1, Cb-B2, and Cd-E1 share the active power delivered to the DC grid, which is the summation of the power generated by wind farms C and D and that imported from AC grid A. The

TABLE II
LINE DATA

	R [Ω/km]	L [mH/km]	C [μF/km]	G [μF/km]	$I_{\max}$ [A]
DC OHL ± 400 kV	0.0114	0.9356	0.0123	–	3500
DC Cable ± 400 kV	0.0095	2.1120	0.1906	0.048	2265
AC cable 145 kV	0.0843	0.2526	0.1837	0.041	715
AC OHL 380 kV	0.0200	0.8532	0.0135	–	3555

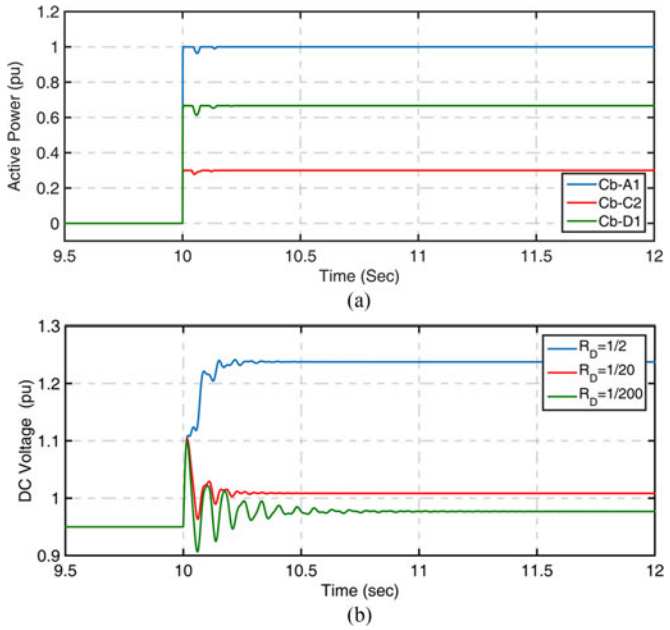

Fig. 8. Changes in droop gains: (a) Step change in the input converter power. (b) Effect of the droop gain values on the DC voltage dynamics.

DSC3 grid buses are thus divided into three types of buses: three power output buses (B1, B2, and B3); three power input buses (B4, B5, and B6); and one connection bus (B7). To achieve this sharing scheme, the proposed supervisory controller selects and sends the optimal droop parameters (i.e., R_{D} and V_{o}) to converters Cb-B1 and Cb-B2 and to the Cd-E1 voltage-droop controller.

A. *Effects of Changing Droop Gains*

To derive the state-space model, the modeling steps explained in Section III were followed. Fig. 8(b) shows the effects of the droop-gain value on the DC voltage dynamics due to a step change in the input power (Fig. 8(a)), based on the assumption that all droop-control converters have the same R_D with $V_o = 0.95$. Increasing the value of the droop gain tends to improve the transient performance of the DC voltage; however, the deviation in the steady state voltage increases and may violate voltage limits.

The small-signal stability study shows the system to be stable for all positive droop gain values and indicates that the system eigenvalues become increasingly negative as the droop gains rise, thus improving transient performance, as shown in Fig. 9. The supervisory controller selects the optimal droop gain

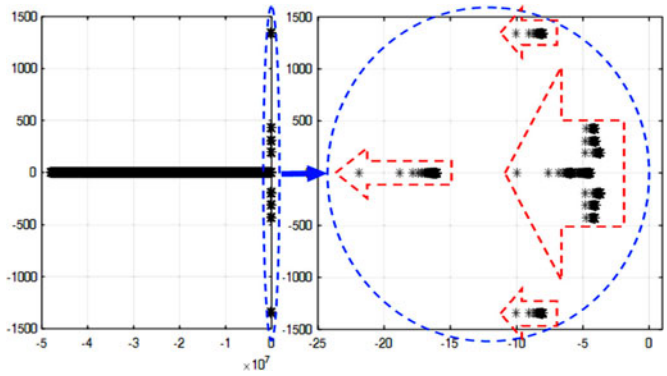

Fig. 9. Movement of the eigenvalues due to the R_{D} incremental from 0.001 to 1.

TABLE III
OPTIMUM DROOP GAIN VALUES

$V_{o\max}$ [p.u.]	Cb-B1	Cb-B2	Cd-E1
1	0.01232	0.01249	0.01249
0.95	0.05970	0.05006	0.06697

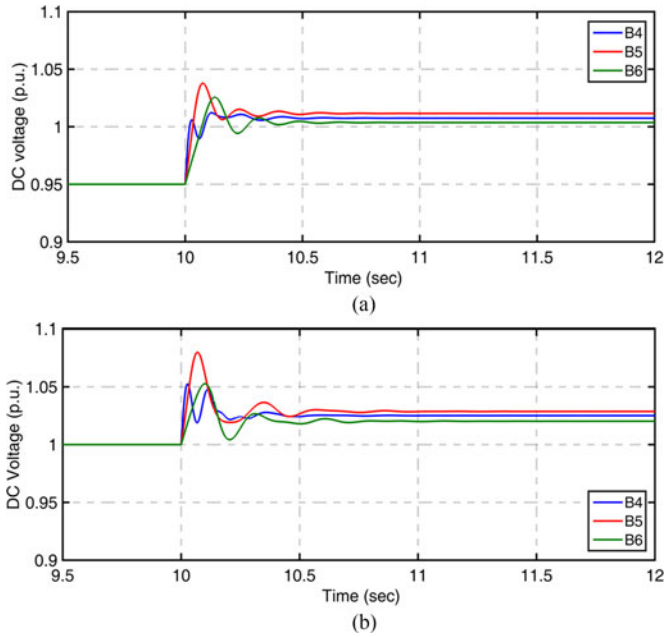

Fig. 10. DC voltages of the input buses: (a) $V_{o_{\max}} = 0.95$; (b) $V_{o_{\max}} = 1$.

for the system by setting the maximum change in the input currents to equal the p.u. rated power values of the power input converters, so $\Delta I_{\max} = [1,\ 0.666,\ 0.334]^T$ p.u. The optimal droop gains at two different $V_{o_{\max}}$ values are shown in Table III. As indicated in Fig. 10, selecting a lower $V_{o_{\max}}$ value results in higher droop gain values, and thus more accurate power sharing with an enhanced dynamic response, all without violating the DC voltage limits at the power input buses.

Fig. 12 shows the DC voltage transient response after a converter outage in the Cb-E1 converter at second 10 as shown in Fig. 11. In this case, all power input converters deliver their

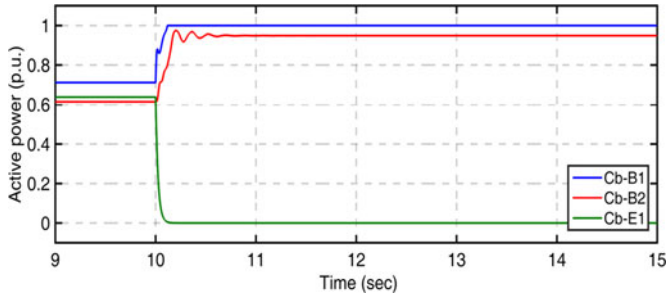

Fig. 11. Active power pf onshore power output converters during a converter outage.

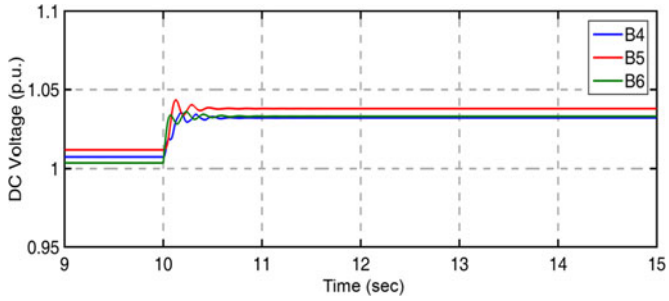

Fig. 12. DC voltage transient response during a converter outage.

TABLE IV
POWER FLOW RESULTS FOR THE BASE CASE SCENARIO

DC Bus	Bus Type	Droop Parameters (R_D , V_o)	Voltage [p.u.]	Power [p.u.]	Power share percentage n
B1	Droop	0.0305, 0.9635	0.98145	−0.5885	29.99%
B2	Droop	0.0500, 0.9401	0.97042	−0.5885	29.99%
B3	Droop	0.0273, 0.9587	0.98058	−0.7847	40.02%
B4	P	–	0.99600	1	–
B5	P	–	0.99975	0.6667	–
B6	P	–	0.99113	0.3333	–
B7	Connection	–	0.97820	–	–

rated power. The droop parameters of the output converters are set at $V_o = 0.95$ p.u. and the R_D droop gains at the values that are listed in Table III. As can be seen in Fig. 12, the selected droop gains by the droop gain selection methodology prevented the DC voltage from exceeding the upper limit.

B. Power-Sharing Base Case

In this case, the active power delivered to the DC network by power input converters Cb-A1, Cb-C2, and Cb-D1 is equal to their rated power. The imported active power is shared among Cb-B1, Cb-B2, and Cd-E1 according to the desired percentage-shares of 30%:30%:40%, respectively. Their droop gains are set as in Table III, with $V_{o_{max}} = 0.95$ p.u. Based on the available input power, desired shares, and droop-gain values, the proposed supervisory controller selects the optimal voltage reference for the power output controllers in order to achieve accurate power sharing. Table IV summarizes the results of the power flow for this case scenario. As can be seen, the optimal no-load voltage values produce actual power shares that are very close to the desired shares, while the DC voltage levels of the HVDC network are maintained within the recommended limits. The results reveal that the proposed control strategy provided accurate power-sharing control based on the desired sharing scheme.

TABLE V
POWER FLOW RESULTS AFTER CHANGING THE INPUT POWER WITH AND WITHOUT OPTIMAL NO-LOAD VOLTAGE VALUES

DC Bus	Non-optimal				Optimal			
	V_o	V [p.u.]	P [p.u.]	n	V_o	V [p.u.]	P [p.u.]	n
B1	0.9311	0.9692	0.3549	26.97%	0.9327	0.9748	0.3946	29.98%
B2	0.9101	0.9611	0.4092	31.09%	0.9183	0.9672	0.3946	29.98%
B3	0.9920	0.9692	0.5518	41.93%	0.9199	0.9751	0.5271	40.04%
B4	–	0.9782	0.5000	–	–	0.9838	0.5000	–
B5	–	0.9822	0.5000	–	–	0.9879	0.5000	–
B6	–	0.9773	0.3333	–	–	0.9832	0.3333	–
B7	–	0.9666	–	–	–	0.9724	–	–

However, if the input power to the HVDC system is changed and the no-load voltage values are not updated to the optimal values, the power sharing control accuracy will be deteriorated and the deviation of the actual power shares from the desired shares will increase. Table V shows a power sharing scenario with different input power. Two cases are considered: the first case is without optimizing the droop controller no-load voltage values after the input power diversion from the base case scenario values. The second case is updating the no-load voltage values corresponding to the new input power. The new input power are 0.5, 0.5, and 0.333 p.u. for VSCs Cb-A1, Cb-C2 and Cb-D1, respectively. The droop gains of the droop controllers are kept the same as the base case scenario. As can be concluded from the percentage shares (n) of the case of using non-optimal parameters and percentage shares (n) of the optimal parameter case in Table V, which represent, the actual percentage shares of both cases, the accuracy of the power sharing control worsened when the droop controller no-load voltage values are not updated. This findings demonstrates the importance of the proposed control strategy in improving the accuracy of power sharing.

C. Sharing of Variable-Input-Power Case

This case demonstrates the ability of the control strategy to deal with input power caused by fluctuations in offshore wind farm generation or surplus power from AC grid A. Fig. 13 shows random variable power imported from wind farms C2 and D1 and from AC grid A. Converters Cb-B1, Cb-B2, and Cd-E1 share power according to the same sharing scheme as in the base case, 30%:30%:40%, respectively. The no-load voltage values of the droop controlled VSCs were calculated and updated every 1 second based on the droop gains listed inTable III at V_{omax} = 0.95 p.u. As can be seen in Fig. 14, the active power sharing among the output converters Cb-B1, Cb-B2, and Cd-E1 follows the desired percentage shares. At any instant, the sharing ratio is fixed, and because of transmission losses in the DC network, the total output power is slightly less than the total input power. The DC voltage level at all DC buses is within limits, as indicated in

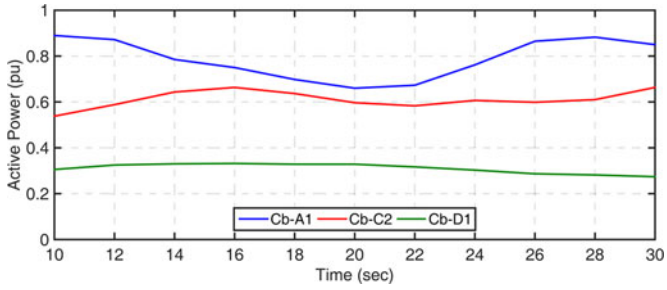

Fig. 13. Variations in input power.

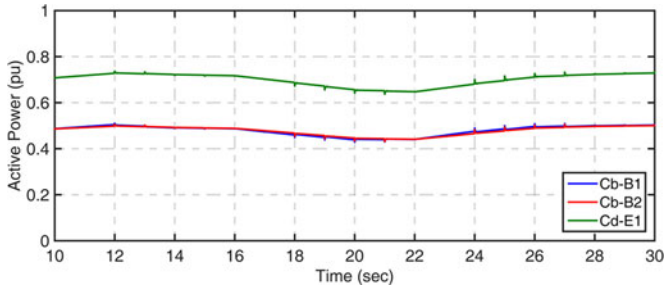

Fig. 14. Power sharing between output converters.

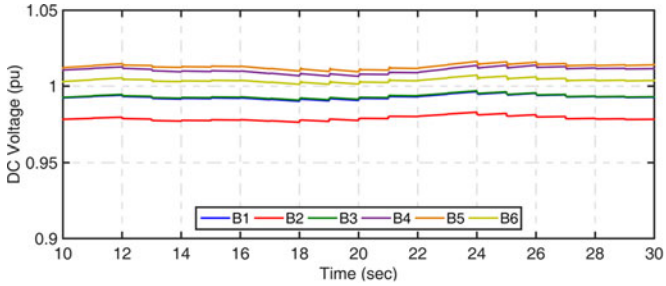

Fig. 15. DC voltages of the buses with power variations.

Fig. 15. These results shows the effectiveness of the proposed control strategy in improving the accuracy of the power sharing in the case of variable input power.

VI. Conclusion

This paper has proposed an OPF-based adaptive voltage-droop control strategy based on predefined desired power shares for power-sharing control and voltage regulation in MT VSC-HVDC networks. The strategy is a two-layer hierarchal control structure. The primary level of the power output converters, which share the incoming power, includes an adaptive voltage-droop controller whose droop-gain and reference-voltage parameters are selected by the supervisory controller in order to achieve specific objectives: enhancing DC voltage dynamics and arriving at an accurate ratio for power-sharing control. To meet these objectives, an optimum droop-gain selection methodology, which includes consideration of the enhancement of DC voltage dynamics, is proposed as a means of improving the transient response of the DC voltage to changes in the input power without violating voltage limits. Optimal droop-reference voltages are then established by the proposed DC OPF-based power-sharing control algorithm.

In all of the simulation results, the proposed control strategy determined an accurate ratio of power-sharing control, thus eliminating the drawbacks associated with conventional voltage-droop control.

TABLE VI
Parameters of the System VSCs Local Controllers

VSCs	Control mode	Inner control loop		Outer control loop	
		K_I	K_i	K_p	K_i
Cb-A1	Droop	0.83	50	–	–
Cb-B1	Droop	0.83	50	–	–
Cb-B2	Droop	0.83	50	–	–
Cb-C2	AC voltage	0.83	50	1	20
Cb-D1	AC voltage	0.83	50	1	20

Appendix A

The Converters Cb-A1, Cb-B1 and Cb-B2 are operating in constant active and reactive power mode, and their controllers consist of one control loop for controlling the dq components of the AC current as shown in Fig. 2. On the other hand, wind farm VSCs: Cb-C2 and Cb-D1 control the AC voltage level of their wind farm AC grids, and their controllers have two cascaded control loops. The inner loop controls the dq components of the AC current components, while the outer loop controls the dq components of the AC voltage. Table VI illustrates the controller parameters of the inner and outer control loops of the systems VSCs that are used in the simulation.

References

[1] L. Xu, L. Yao, and C. Sasse, "Grid integration of large DFIG-based wind farms using VSC transmission," *IEEE Trans. Power Syst.*, vol. 22, no. 3, pp. 976–984, Aug. 2007.
[2] European Transmission System Operators, "European wind integration study (EWIS) towards a successful integration of wind power into European electricity grids-final report," European Transmission System Operators, Brussels, Belgium, 2007.
[3] K. Rudion and A. G. Orths, "Offshore power system operation planning considering energy market schedules," *IEEE Trans. Sustain. Energy*, vol. 4, no. 3, pp. 725–733, Jul. 2013.
[4] Y. Tokiwa, F. Ichikawa, and K. Suzuki, "Novel control strategies for HVDC system with self-contained converter Tokyo Electric Power Co.," *Electr. Eng. Japan*, vol. 113, no. 5, pp. 1–13, 1993.
[5] R. Teixeira Pinto, S. F. Rodrigues, P. Bauer, and J. Pierik, "Comparison of direct voltage control methods of multi-terminal DC (MTDC) networks through modular dynamic models," in *Proc. 14th Eur. Conf. Power Electron. Appl.*, 2011, pp. 1–10.
[6] C. Dierckxsens, K. Srivastava, M. Reza, S. Cole, J. Beerten, and R. Belmans, "A distributed DC voltage control method for VSC MTDC systems," *Electr. Power Syst. Res.*, vol. 82, no. 1, pp. 54–58, Jan. 2012.
[7] F. Gonzalez and J. Roldan, "Effects of DC voltage control strategy on voltage response on multi-terminal HVDC following loss of a converter station," in *Proc. IEEE Power Energy Soc. Gen. Meet.*, 2013, pp. 1–5.
[8] K. Rouzbehi, S. Member, A. Miranian, J. I. Candela, A. Luna, and P. Rodriguez, "A generalized voltage droop strategy for control of multi-terminal DC grids," *IEEE Trans. Ind. Appl.*, vol. 51, no. 1, pp. 607–618, Jan./Feb. 2015.
[9] R. T. Pinto, P. Bauer, S. F. Rodrigues, E. J. Wiggelinkhuizen, J. Pierik, and B. Ferreira, "A novel distributed direct-voltage control strategy for grid integration of offshore wind energy systems through MTDC network," *IEEE Trans. Ind. Electron.*, vol. 60, no. 6, pp. 2429–2441, Jun. 2013.

[10] L. Xu, L. Yao, and M. Bazargan, "DC grid management of a multi-terminal HVDC transmission system for large offshore wind farms," in *Proc. 2009 Int. Conf. Sustain. Power Gener. Supply*, Apr. 2009, pp. 1–7.
[11] O. Gomis-Bellmunt, J. Liang, J. Ekanayake, R. King, and N. Jenkins, "Topologies of multiterminal HVDC-VSC transmission for large offshore wind farms," *Electr. Power Syst. Res.*, vol. 81, no. 2, pp. 271–281, Feb. 2011.
[12] M. Aragüés-Peñalba, A. Egea-Àlvarez, S. G. Arellano, and O. Gomis-Bellmunt, "Droop control for loss minimization in HVDC multi-terminal transmission systems for large offshore wind farms," *Electr. Power Syst. Res.*, vol. 112, pp. 48–55, Jul. 2014.
[13] A. S. Abdel-khalik, S. Member, A. M. Massoud, A. A. Elserougi, and S. Ahmed, "Optimum power transmission-based droop control design for multi-terminal HVDC of offshore wind farms," *IEEE Trans. Power Syst.*, vol. 28, no. 3, pp. 3401–3409, Aug. 2013.
[14] E. Prieto-araujo, F. D. Bianchi, A. Junyent-ferré, and O. Gomis-Bellmunt, "Methodology for droop control dynamic analysis of multiterminal VSC-HVDC grids for offshore wind farms," *IEEE Trans. Power Del.*, vol. 26, no. 4, pp. 2476–2485, Oct. 2011.
[15] T. M. Haileselassie and K. Uhlen, "Impact of DC line voltage drops on power flow of MTDC using droop control," *IEEE Trans. Power Syst.*, vol. 27, no. 3, pp. 1441–1449, Aug. 2012.
[16] X. Zhao and K. Li, "Adaptive backstepping droop controller design for multi-terminal high-voltage direct current systems," *IET Gener. Trans. Distrib.*, vol. 9, no. 10, pp. 975–983, Jul. 2015.
[17] E. Prieto-Araujo, A. Egea-Alvarez, S. (Fekri) Fekriasl, and O. Gomis-Bellmunt, "DC voltage droop control design for multi-terminal HVDC systems considering AC and DC grid dynamics," *IEEE Trans. Power Del.*, vol. 31, no. 2, pp. 575–585, Apr. 2016.
[18] N. R. Chauhuri and B. Chauhudri, "Adaptive droop control for effective power sharing in multi-terminal DC (MTDC) grids," *IEEE Trans. Power Syst.*, vol. 28, no. 1, pp. 21–29, Feb. 2013.
[19] R. Eriksson, J. Beerten, M. Ghandhari, and S. Member, "Optimizing DC voltage droop settings for AC/DC system interactions," *IEEE Trans. Power Del.*, vol. 29, no. 1, pp. 362–369, Feb. 2014.
[20] X. Lu, J. M. Guerrero, K. Sun, and J. C. Vasquez, "An improved droop control method for DC microgrids based on low bandwidth communication with DC bus voltage restoration and enhanced current sharing accuracy," *IEEE Trans. Power Electron.*, vol. 29, no. 4, pp. 1800–1812, Apr. 2014.
[21] M. K. Bucher, R. Wiget, G. Andersson, and C. M. Franck, "Multiterminal HVDC networks—What is the preferred topology?," *IEEE Trans. Power Del.*, vol. 29, no. 1, pp. 406–413, Feb. 2014.
[22] J. Beerten, S. Cole, and R. Belmans, "Modeling of multi-terminal VSC HVDC systems with distributed DC voltage control," *IEEE Trans. Power Syst.*, vol. 29, no. 1, pp. 34–42, Jan. 2014.
[23] G. Pinares, L. B. Tjernberg, L. A. Tuan, C. Breitholtz, and A.-A. Edris, "On the analysis of the DC dynamics of multi-terminal VSC-HVDC systems using small signal modeling," in *Proc. 2013 IEEE Grenoble Conf.*, Jun. 2013, pp. 1–6.
[24] J. Beerten and R. Belmans, "Modeling and control of multi-terminal VSC HVDC systems," *Energy Procedia*, vol. 24, pp. 123–130, Jan. 2012.
[25] G. O. Kalcon, G. P. Adam, O. Anaya-Lara, S. Lo, and K. Uhlen, "Small-signal stability analysis of multi-terminal VSC-based DC transmission systems," *IEEE Trans. Power Syst.*, vol. 27, no. 4, pp. 1818–1830, Nov. 2012.
[26] J. Peralta, H. Saad, and S. Dennetière, "Detailed and averaged models for a 401-Level MMC–HVDC system," *IEEE Trans. Power Del.*, vol. 27, no. 3, pp. 1501–1508, Jul. 2012.
[27] T. M. Haileselassie and K. Uhlen, "Power flow analysis of multi-terminal HVDC networks," in *Proc. 2011 IEEE Int. Conf. Trondheim PowerTech*, Jun. 2011, pp. 1–6.
[28] S. Skogestad and I. Postlethwaite, *Multivariable Feedback Control Analysis and design*. New York, NY, USA: Wiley, 2005.
[29] G. A. Shultzt, "A trust region algorithm for nonlinearly constrained optimization," *SIAM J. Numer. Anal.*, vol. 24, no. 5, pp. 1152–1170, 1987.
[30] CIGREE B4 Working Group, "The CIGRE B4 DC grid test system," 2013. [online] Available: http://b4.cigre.org/Publications/Documents-related-to-the-development-of-HVDC-Grids

Mohamed Abdelaziz Abdelwahed (S'14) was born in Cairo, Egypt, on 1981. He received the B.Sc. and M.Sc. degrees from Faculty of Engineering, Benha University, Benha, Egypt, in 2003 and 2010, respectively. He is currently working toward the Ph.D. degree in electrical and computer engineering at the University of Waterloo, Waterloo, ON, Canada. He is an Assistant Lecturer in the Department of Electrical Engineering and on study leave in University of Waterloo. His Ph.D. scholarship is funded by the Faculty of Engineering, Benha University. His research interests include multiterminal HVDC transmission systems.

Ehab F. El-Saadany (SM'05) was born in Cairo, Egypt, on 1964. He received B.Sc. and M.Sc. degrees in electrical engineering from Ain Shams University, Cairo, Egypt, in 1986 and 1990, respectively, and the Ph.D. degree in electrical engineering from the University of Waterloo, Waterloo, ON, Canada, in 1998. He is currently a Professor in the Department of Electrical and Computer Engineering, University of Waterloo, and currently on leave with the Petroleum Institute, Abu Dhabi, UAE. His research interests include smart grid operation and control, power quality, distributed generation, power electronics, digital signal processing applications to power systems, and mechatronics. Dr. El-Saadany is Canada Research Chair in Smart Distribution Systems, an Editor of the IEEE TRANSACTIONS ON SMART GRID, and a Registered Professional Engineer in the Province of Ontario.